




Photo-sensing properties of Cd-doped In_2S_3 thin films fabricated via low-cost nebulizer spray pyrolysis technique

S. Rajeswari¹, M. Mohamed Ibrahim^{1,*}, Abdullah M. Al-Enizi², Mohd Ubaidullah^{2,*} , Prabhakarn Arunachalam², Bidhan Pandit³, and Shoyebmohamad F. Shaikh²

¹Department of Physics, Kongunadu Arts and Science College, Coimbatore, India

²Department of Chemistry, College of Science, King Saud University, Riyadh 11451, Saudi Arabia

³Department of Materials Science and Engineering and Chemical Engineering, Universidad Carlos III de Madrid, Avenida de la Universidad 30, 28911 Leganés, Madrid, Spain

Received: 7 January 2022

Accepted: 12 July 2022

Published online:

8 August 2022

© The Author(s), under exclusive licence to Springer Science+Business Media, LLC, part of Springer Nature 2022

ABSTRACT

In this study, we report the fabrication of cadmium-doped indium sulfide thin films ($\text{In}_2\text{S}_3\text{:Cd}$) using a low-cost nebulizer-aided spray pyrolysis process at 350 °C on glass substrates for photo-sensing applications. The impact of 0, 2, 4, and 8 wt% cadmium concentrations on the structure, morphology, optical properties, and photo-sensing capabilities of In_2S_3 thin films were examined systematically. From X-ray diffraction (XRD) analysis, the major peak is located in the (103) plane for all Cd-doped In_2S_3 thin film samples, and the maximum crystallite size for the 4 wt% sample is 59 nm. The field emission scanning electron microscope (FESEM) image revealed a homogenous large-grained surface of Cd-doped In_2S_3 film that completely covered the substrate. UV–Vis absorption analysis demonstrated good absorption for all thin film samples in the visible and ultraviolet regions of the electromagnetic spectrum, particularly, the 4% Cd-doped concentration showed excellent absorption as is observed from Tauc relation. The highest PL intensity at 680 nm was observed for the sample coated with 4 wt% of Cd. Under UV light, the I – V behavior depicts a light current of 1.06×10^{-6} A for a 5 V bias voltage. The $\text{In}_2\text{S}_3\text{:Cd}$ (4%) sample had the highest responsivity of 2.12×10^{-1} A/W and a detectivity of 1.84×10^{11} Jones, with a high EQE of 50%. The study manifests that the developed Cd (4%)-doped In_2S_3 thin film sample might be better suited for the application of photodetectors.

Address correspondence to E-mail: mibrahim27@gmail.com; mtayyab@ksu.edu.sa

1 Introduction

In recent years, thin films have received significant interest owing to their prospective applications in various optoelectronic and electronic devices. Because of their intriguing physical features, n-type In_2S_3 semiconductor thin films have recently received a lot of attention towards light-emitting diodes (LEDs), photodetectors, solar cells, and other optoelectronic applications [1–8]. Various synthesis procedures including electro-deposition [2], vacuum evaporation [9], successive ionic layer absorption and reaction (SILAR) [10], CBD [11], pulse electro-deposition [12], hot wall epitaxial method [13, 14], hydrothermal [15], and nebulizer spray pyrolysis [16–18] have been used to develop indium sulfide thin films. Nonetheless, fabricating a device quality In_2S_3 material onto a substrate using a low-cost technique remains a challenge. Indium sulfide acts as a crucial compound in optoelectronic and photovoltaic applications [19–21] because of its stability, broader energy gap, and photoconductive behavior [22]. It also possesses fascinating photoluminescence characteristics [23], making it suitable for a wide range of optoelectronic applications [24]. Doping is an effective way to improve the physical properties of the semiconducting materials. Addition of dopants could effectively alter the energy gap of the semiconductors facilitating the electron transport from the ground state to excited state. Various transition metal dopants have been previously studied to change the structural and electrical properties of In_2S_3 films. Doping of In_2S_3 films with Sn exhibits lower resistance, according to Becker et al. [25]. Kim et al. found that doping cobalt into single crystals of indium sulfide reduces structural flaws [26]. According to Kamoun et al., the addition of Al increased the oxygen adsorption in the sample [27]. Diehl and Nitsche [28] studied the stability of In_2S_3 thin films by replacing the In atoms with Bi, As, Sb, or Zn. According to Barreau et al. [29], adding Na resulted in a wider bandgap and enhanced conductivity. In our study, we have investigated the effect of Cadmium (Cd) doping on the physical properties of the In_2S_3 films. Moreover, the ionic radius of Cd^{2+} (0.95 Å) is larger compared to the ionic radius of In^{3+} (0.80 Å) which could result in the formation of favorable imperfections in the In_2S_3 lattice. Generally, Cd dopant alters the bandgap of the semiconducting

materials, and it would be exciting to study their impact on the In_2S_3 for photo-sensing applications.

Physical deposition processes are relatively expensive and energy intensive, while producing high-quality and homogenous films. The nebulizer spray pyrolysis process (NSP) is a simple and cost-effective method for producing thin films efficiently. The NSP approach has been used to deposit ternary and binary oxide base semiconducting thin films such as MgO [30], tin-doped zinc oxide [31], Y-doped NiO [32], Zn-doped Cu_2O [33], and Cd-doped SnO_2 [34]. This approach was also used to deposit ternary chalcogenide cadmium-tin-selenium (CdSnSe) thin film [35]. While the NSP method for thin film synthesis has been extensively employed to generate a range of thin films, there were no investigations on the fabrication of Cd-doped In_2S_3 thin films. Hence, in this work, we report Cd-doped In_2S_3 thin films grown using nebulizer spray pyrolysis on glass substrates and the thin films have been studied for their optical, structural, morphological, elemental, and photo-sensing properties.

2 Experimental technique

2.1 Fabrication of Cd-doped In_2S_3 thin films

Cd-doped In_2S_3 thin films were developed on soda-lime glass (SLG) substrates using the cost-effective NSP process. The chemicals InCl_3 , CdCl_2 , and NH_2CSNH_2 were purchased from Sigma-Aldrich with a purity of 99.99%. Before the start of the deposition process, the SLG substrates were subjected to standard procedures to remove the substrate impurities. The substrates were dipped in chromic acid and then washed multiple times with a hot soap solution before being cleaned with DI water. After the cleaning process, the sample was placed in the NSP unit holder with a 2.5 cm × 2.5 cm dimension. To generate the spray solution, 0.2 M of indium chloride (0.442 g) and 0.3 M of thiourea (0.228 g) were used as precursors and liquefied in 10 mL double-filtered water. The precursor solution's doping content was adjusted to 0, 2 (0.003 g), 4 (0.007 g), 6 (0.014 g), and 8 wt% (0.029 g) in 2 wt% increments. To make a homogenous mixture, the precursor solution was agitated on a hot plate for 30 min with a magnetic pellet. The precursor solution was then filled in the

NSP unit's nebulizer container for deposition. To make fine aerosol droplets, the air is employed as a bearer gas with a pressure of 1.5 kg/cm^2 [36]. During the deposition, the conditions maintained are spray rate of 1 mL/min , 10 min time of deposition, the distance between the substrate and nozzle was kept as 5 cm, and the temperature was maintained at $350 \text{ }^\circ\text{C}$. The chemical reaction of the In_2S_3 formation is

$$2\text{InCl}_3 + 3\text{SC}((\text{NH}_2)_2) \rightarrow \text{In}_2\text{S}_3(\text{s}) + 6\text{HCl}(\text{g}) + 3\text{H}_2\text{NCN}(\text{g})$$
 [37]. Following deposition, the thin films were left uninterrupted in the film deposition chamber until they reached room temperature, after which they were removed for further investigations.

2.2 Characterization techniques of Cd-doped In_2S_3 thin films

The structure, shape, content, and light detecting characteristics of the prepared films were investigated utilizing various analytical approaches. Using the wavelength of 0.15406 nm for the source and a voltage range of around 40 kV , an X-ray diffractometer (PANalytical X'Pert Pro) was used to inspect the structural parameters of the produced Cd-doped In_2S_3 thin films. A field emission scanning electron microscope (Zeiss) was used to examine the texture of the film's surface. The elemental composition of the films was determined using the appended EDX. To evaluate the optical characteristics of the prepared thin films, a UV-Vis spectrometer (PerkinElmer 4 Lambda 35) was used in the wavelength range of $300\text{--}900 \text{ nm}$. A fluorescence spectrometer (PerkinElmer LS-55) was utilized to study the room temperature PL spectra, and a Keithley 2450 model source meter with 365 nm laser source was used to assess the photo-sensing parameters.

3 Results and discussion

3.1 Structural analysis

Figure 1 shows the X-ray diffraction patterns of pristine and Cd-doped In_2S_3 thin films formed at $350 \text{ }^\circ\text{C}$ with various Cd doping concentrations. The inter-planar spacing " d " values for the distinct peaks in the patterns were calculated and compared with standard values according to the (JCPDS 88-0287). The polycrystalline character of the thin films along

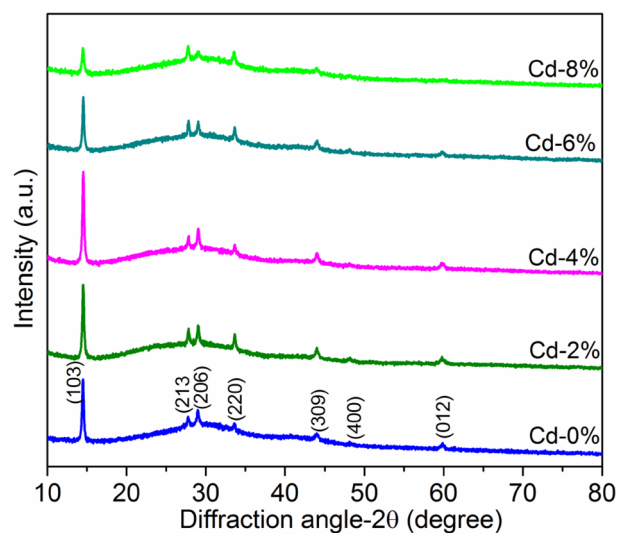


Fig. 1 XRD patterns of Cd-doped In_2S_3 thin films

with the tetragonal structure is revealed by X-ray diffraction patterns. Additional peaks were recorded at the (213), (206), (220), (309), (400), and (012) planes, with the most intense peak being observed along the (103) plane. The maximum peak intensity of the (103) plane increased steadily when the Cd doping concentration was increased from 0 to 4% due to increased crystallinity, as shown in Fig. 1. The strength of the diffraction peaks decreases as the Cd doping concentration rises above 4%, showing crystallinity loss due to lattice distortion. It confirms that the Cd: In_2S_3 doping concentration has a significant impact on the crystalline and film quality.

Crystallite size D in the films as well as the existing microstrain were calculated using size-strain plot [38] (Fig. S1). Table 1 shows that as the doping concentration increases, the crystallite size value increases. This increase in crystallite size is attributed to the rise in nucleation on the coating surface as a result of grain boundary migration caused by a drop in the film's surface energy [39]. The relationship can be used to find the strain in the prepared films. The predicted microstrain in the films decreased as the doping concentration increased up to 4%, most likely due to a decrease in cohesion between the In_2S_3 film and the coating surface [39].

3.2 Morphological analysis

FESEM is a beneficial technique for studying the surface morphology of films and provides valuable information on the size and morphology of the

Table 1 Structural parameters and bandgap of Cd-doped In₂S₃ thin films

Cd doping concentration (%)	Crystallite size (nm)	Strain × 10 ⁻³	Bandgap (eV)
0	33	5.70	2.86
2	37	3.66	2.93
4	39	3.51	2.98
6	37	2.37	2.82
8	29	5.39	2.69

particles or grains. Figure 2 shows the surface morphology of pure and Cd-doped In₂S₃ thin films deposited at 350 °C. From the figure, it was observed that the developed pure and Cd-doped In₂S₃ thin films exhibit homogeneous distribution of the crystallites strewn with microscopic flakes or crystal clusters in the nanometer range. It was also noted that the crystallization increases with the increase in concentration of the Cd dopants up to 4% and the In₂S₃:Cd (4%) film exhibits better crystallization. Further, introduction of the Cd dopants in In₂S₃ above 4% leads to deterioration in the crystals due to lattice distortion as confirmed by our XRD results, which shows an uneven/decrease in crystal morphology in the case of In₂S₃:Cd (6% & 8%) films. The nano-sized flake and sphere-shaped crystal structures have almost vanished, leaving only tiny clusters observed throughout the films, inferring the changes in the size and shape of the grains due to higher order Cd doping. Figure 2f shows the characteristic EDX spectrum of Cd-doped In₂S₃ thin film produced at a doping concentration of 4%. It revealed the existence of S, In, and Cd as elementary components and revealed their distinct composition and purity. The additional peaks in the EDX spectrum might be due to the presence of substrate impurities.

3.3 Optical analysis

Figure 3 shows the optical absorbance spectra of Cd-doped In₂S₃ thin films sprayed with a nebulizer in the range of wavelength (300–900 nm). When the doping concentration was raised, the absorption seemed to increase. When the doping concentration is raised, idealized energy levels are produced within the bandgap, raising light immersion and, as a result, lowering its transmittance. Using the formula [40], the absorption coefficient was obtained.

$$\alpha = \frac{1}{d} \ln\left(\frac{1}{T}\right) \tag{1}$$

The thickness of the films is denoted by d, while the amount of transmittance is denoted by T. When compared to the other films, the sample made with a 4% Cd-doped film has a higher absorption. The bandgap values may be estimated using the Tauc’s relation and the computed absorption parameter values, as well as the direct allowed optical transition of Cd-doped In₂S₃ [41].

$$\alpha hv = A(hv - E_g)^n \tag{2}$$

The photon’s incident energy is hv, the proportionality constant is A, and the value of n is 1/2. The linear part of the generated curves was straightly fit over the X-axis after a graph was drawn between αhv along the Y-axis and hv along the X-axis. Figure 3 depicts the Tauc plots. As the Cd doping concentration increased from 0% to 8%, the bandgap energy changed from 2.86 to 2.69 eV. The bandgaps calculated were alike to those reported by Thierno Sall et al. [42] and Teny Theresa John et al. [43], but they were much greater than the pure sample value of 2.10 eV [44] due to oxygen incorporation during film manufacturing or an excess of sulfur in the lattice [45]. It could also be due to the variations in the films’ stoichiometry, preference orientation in the film, or the quantum size effect [46]. But, in the present work, the bandgap variation is due to the variation in crystallite size and defects of the samples.

3.4 Photoluminescence (PL) analysis

Photoluminescence spectroscopic examination at an excitation wavelength of 450 nm was used to investigate the defect levels in spray-produced Cd-doped In₂S₃ thin films at various Cd doping concentrations and the resulting spectra are presented in Fig. 4. The spectra revealed two emission bands: a red emission and a green emission. Bulk In₂S₃ is not predicted to

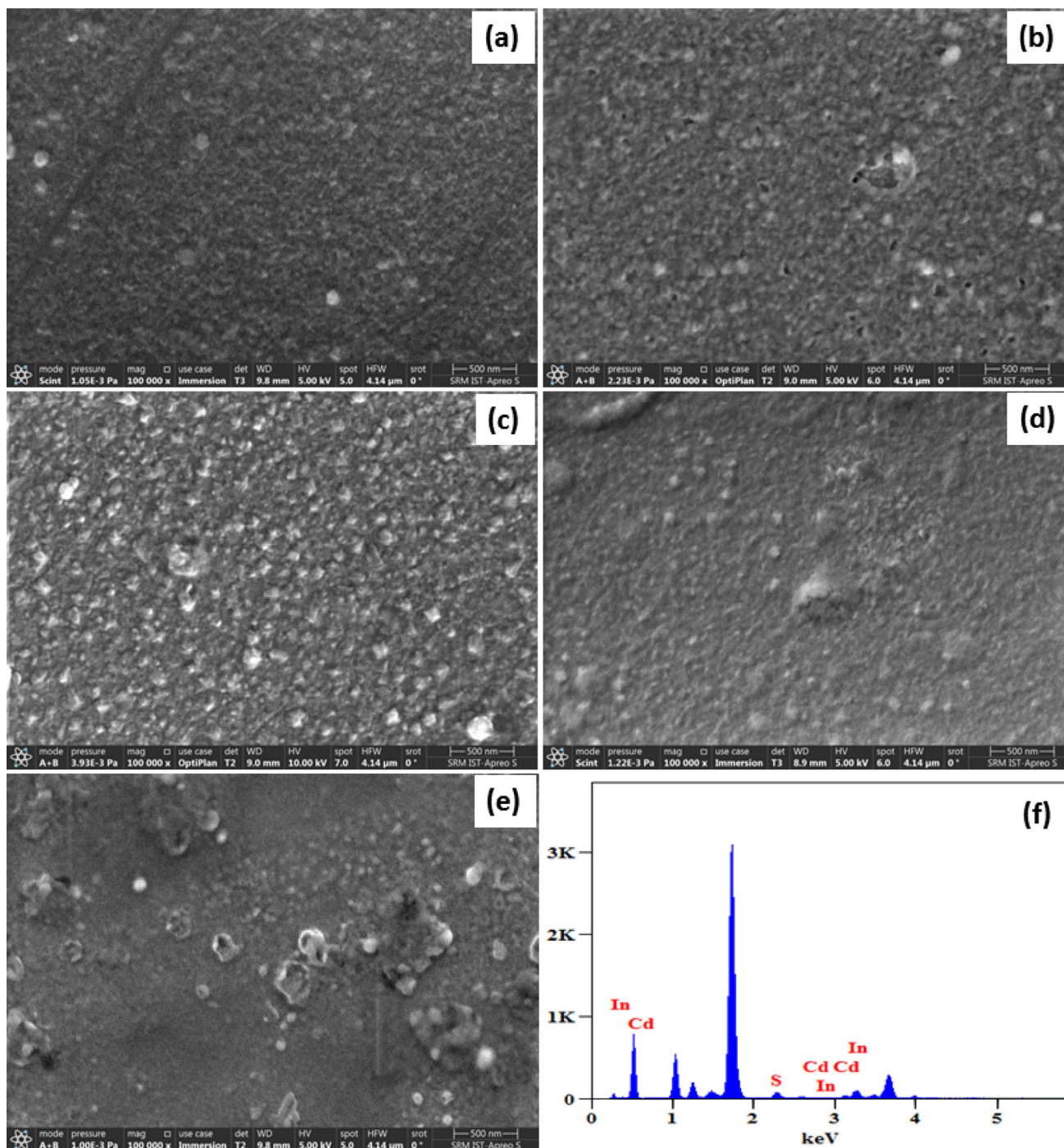


Fig. 2 FESEM images of Cd-doped In_2S_3 thin films. **a** Cd (0%), **b** Cd (2%), **c** Cd (4%), **d** Cd (6%), **e** Cd (8%), and **f** EDX image of In_2S_3 :Cd (4%) thin film

be luminous at ambient temperature. The conversion between donors formed by sulfur vacancies (V_s) and acceptors created by indium vacancies (V_{In}) occurs at 523 nm. Zhao et al. previously discovered this broad peak in In_2S_3 microflakes [47]. The conversion from indium interstitial (I_{In}) donors to oxygen in the

vacancy of sulfur (OVs) acceptors was assigned to the second peak at 680 nm [48], which is more for 4% Cd-doped In_2S_3 thin film. It is worth noting that the creation of oxygen bending defects always opens up new possibilities for improving photoconductive characteristics. The short distance between inter-band

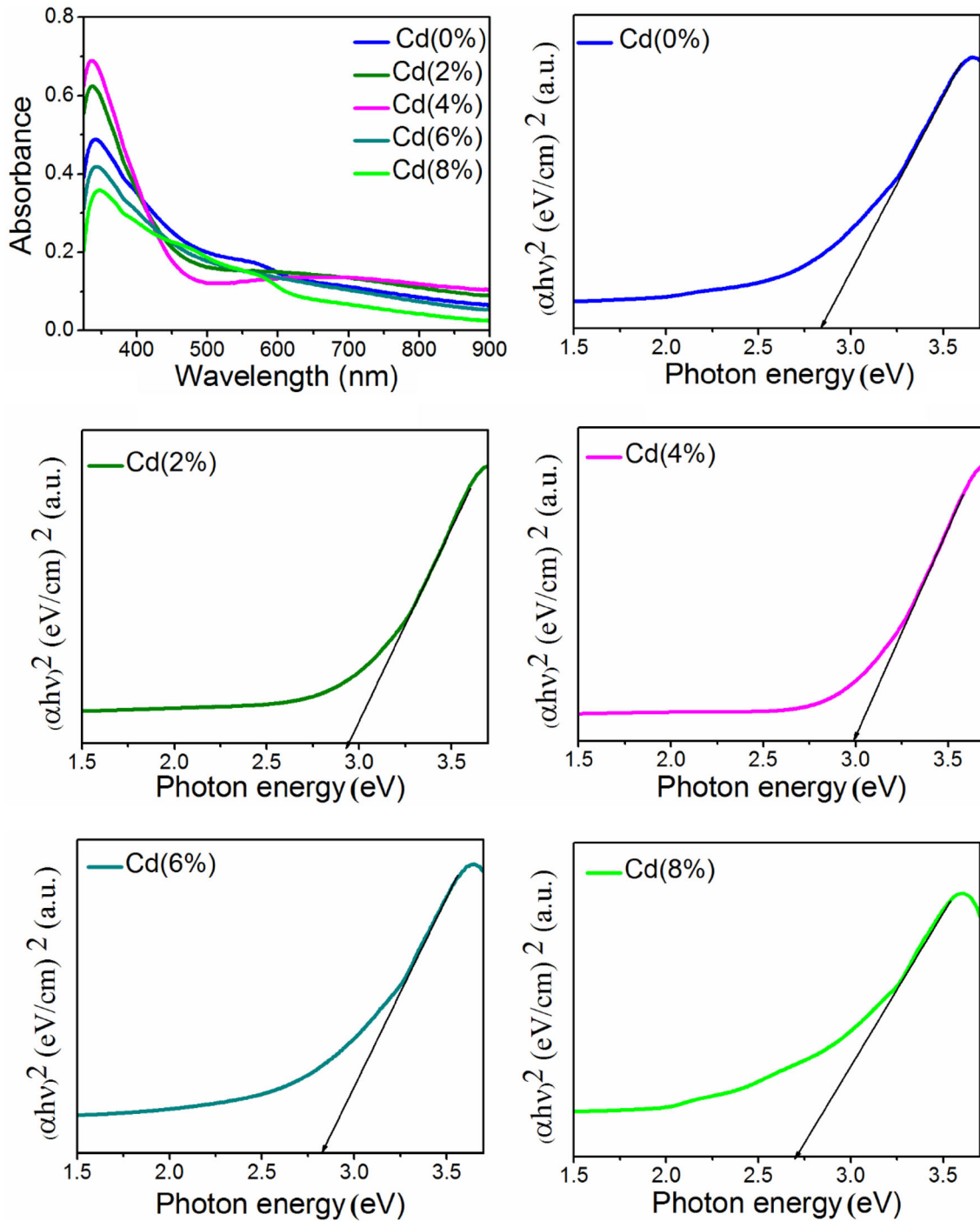


Fig. 3 Absorption spectra and Tauc's plot of Cd-doped In_2S_3 thin films

metal ions results in the increase in charge transfer between neighboring ions, which reduces the PL intensities for higher Cd-doped samples like 6 and 8 wt%.

3.5 I–V characteristics analysis

Cd-doped In_2S_3 films size (1 cm × 1 cm dimensions) with Ag metal coating as the electrode was taken for photo-sensing analysis. Figure 5 shows the V–I feature of the films in light and dark modes with an application of bias voltage ranging from – 5 to 5 V. It

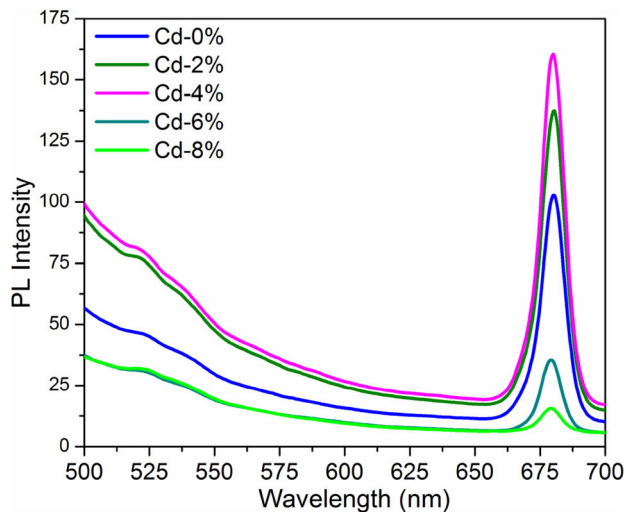
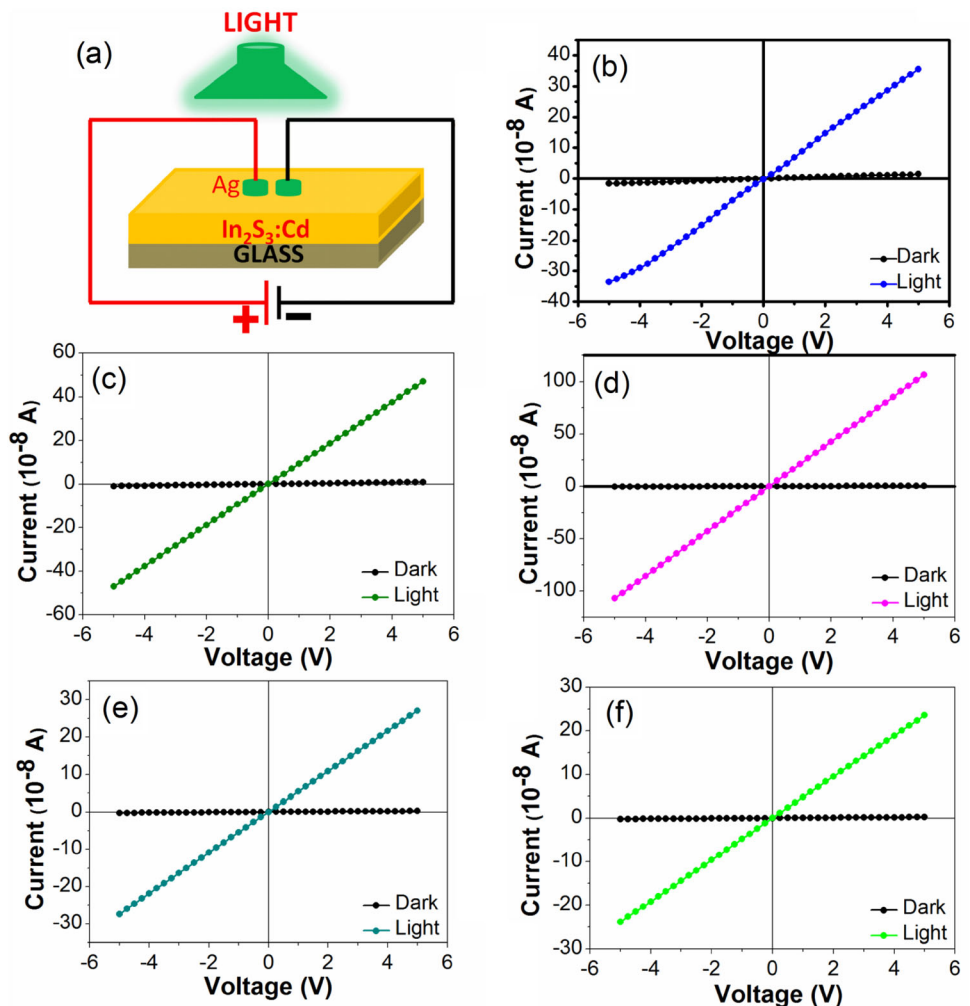


Fig. 4 PL spectra of Cd-doped In_2S_3 thin films

confirms the ohmic nature of all the films. For the same bias voltage, a higher photocurrent is detected for all samples, especially, the 4% Cd concentration In_2S_3 sample showed a photocurrent value of $1.06 \times 10^{-6} \text{ A}$ which is higher compared to other fabricated samples. This determines the deposited films' ability to absorb light and form electron-hole pairs, which then separate and gather, resulting in a rise in current. The measured values of Cd-doped In_2S_3 thin film's photo-sensing parameters like photo-responsivity (R), detectivity (D^*), and external quantum efficiency (EQE) for different doping concentrations are shown in Fig. 6 and tabulated in Table 2. The following equation [49] can be used to find responsiveness.

Fig. 5 **a** Device structure of Cd-doped In_2S_3 thin film photodetector. Transverse I – V characteristics of the deposited Cd-doped In_2S_3 thin films at different doping concentrations in light and dark modes. **b** 0%, **c** 2%, **d** 4%, **e** 6%, **f** 8%



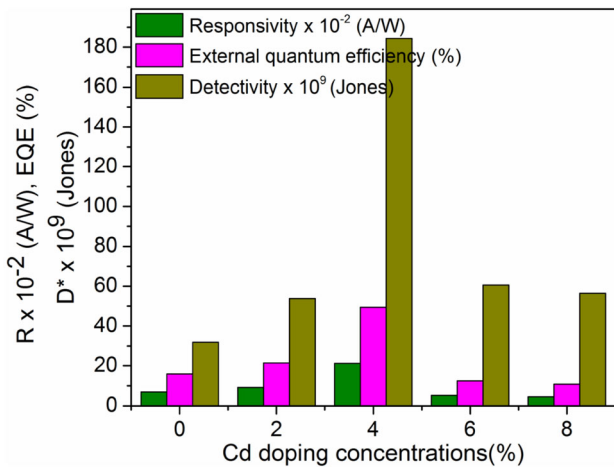


Fig. 6 Responsivity, External quantum efficiency, and detectivity values of the Cd-doped In₂S₃ thin films

$$R = \frac{I_{ph}}{P \times A} \tag{3}$$

The photo-responsivity of detectors was computed by substituting the value of photocurrent I_{ph} , incident light power (P), and the surface area of the thin film (A). The calculated responsivity values were found to increase from 6.81×10^{-2} to 2.12×10^{-1} A/W as doping concentration was raised from 0% to 4%. The measured responsivity is almost similar to that published by Hemanth et al. for an In₂S₃ metal and semiconductor metal photodetector created by co-evaporation approach [50], which was 5.360 mA/W.

The amount of electromagnetic energy converted to useable current is given by the value of EQE, which may be calculated using Eq. (4) [51].

$$EQE = R \frac{hc}{e\lambda} \tag{4}$$

EQE values were computed by substituting the Planck’s constant h , the velocity of electromagnetic wave (c), the incident electromagnetic energy wavelength is (λ), and the charge of an electron (e). When

the doping concentration was raised from 0 to 8%, the EQE values ranged from 16 to 11%. The film doped with 4% showed the highest efficiency of 50%. By using the responsivity value (R), film area A , and dark current I_d in the following equation, the detectivity of the films may be calculated [52].

$$D^* = R \sqrt{\frac{A}{2eI_d}} \tag{5}$$

The pure In₂S₃ film’s detectivity is found to be 3.18×10^{10} Jones. The detectivity of the film improved as the doping ratio of the solution raised. The 4% Cd-doped film had a detectivity of 1.84×10^{11} Jones, which is greater compared with other films. The detectivity values obtained are significantly greater than those previously reported [51]. The transient current characteristics can be used to examine the performance of the Cd-doped In₂S₃ photodetector. Figure 7 depicts the current–time characteristics in determining the photo-response properties of Cd-doped In₂S₃ thin films with varying incident light ranging from 1 to 5 mW/cm². When the UV light is in an ON state, the photocurrent values raises and reach the saturation point, when the light is turned off, the current decreases and returns to its initial state, suggesting that the device is more stable and reversible. The response/recovery time depends on many factors such as type of semiconducting material, operating temperature, suitable dopants, and light intensity. The response time and recovery time for all the samples measured are noted in Table 2. It was observed that the current value increases linearly with the increase in light intensity and higher current value was observed to be 5 mW/cm² for all the photodetector samples. Also, the highest current value and minimum response time/recovery time of 1.6 s/1.3 s were observed for 4% Cd-doped In₂S₃ sample compared to other fabricated photodetectors. The rise in photocurrent with

Table 2 The device performance parameters of fabricated Cd-doped In₂S₃ thin films

Samples	R (AW ⁻¹)	EQE (%)	D* (Jones)	Response time (s)	Recovery time (s)
In ₂ S ₃	6.81E-02	16	3.18E + 10	2.1	1.4
In ₂ S ₃ :Cd(2.0%)	9.19E-02	21	5.38E + 10	1.8	1.5
In ₂ S ₃ :Cd(4.0%)	2.12E-01	50	1.84E + 11	1.6	1.3
In ₂ S ₃ :Cd(6.0%)	5.34E-02	12	6.05E + 10	1.6	1.5
In ₂ S ₃ :Cd(8.0%)	4.66E-02	11	5.64E + 10	1.7	1.4

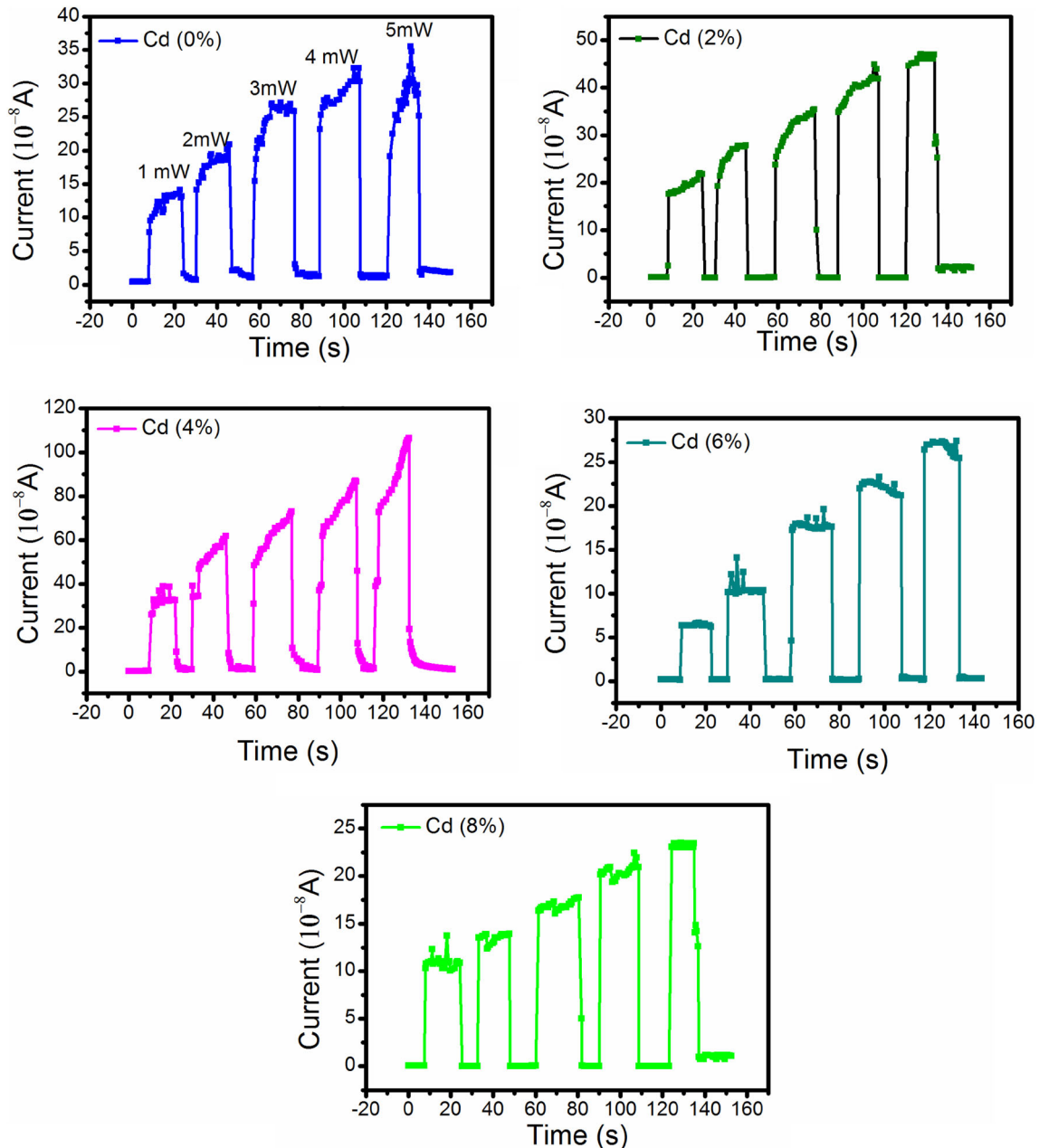


Fig. 7 Transient photo-response characteristics of the Cd-doped In_2S_3 thin films

the increase in light intensities could be attributable to a rise in light-induced carriers and improved electron–hole pair separation due to lesser defects [53]. Further, the decrease in photocurrent and larger response time/recovery time of the 6 and 8% Cd-doped In_2S_3 samples might be because of the induced defects caused due to higher order doping of Cd occupying the interstitial/substitutional sites in In_2S_3 lattice. Table 3 shows a comparison of the current work's photodetector performance with that of

prior CdS and In_2S_3 nanostructures photodetectors [54–59]. The following are the reasons for high photo-response, i.e., broadened absorption and smaller bandgap resulting in more photons being absorbed and an increase in illumination current.

3.6 Photo-sensing mechanism

A photodetector's performance under dark and light illumination can be explained using a variety of techniques. The production of electron–hole pairs is

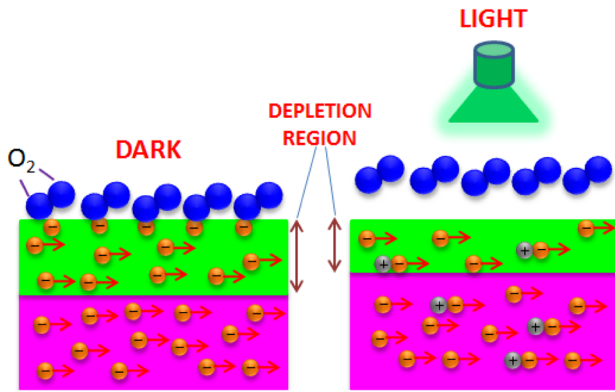


Fig. 8 Schematic diagram of photo-sensing mechanism

critical for improving photocurrent in response to various bias voltages. Figure 8 shows the adsorption and desorption of oxygen at air (before light) and illumination (after light) conditions to better understand the performance of a photodetector. Because $\text{In}_2\text{S}_3:\text{Cd}$ belongs to the broad bandgap semiconducting group, the photo-sensor is investigated using UV light. The oxygen molecules adsorbed on the $\text{In}_2\text{S}_3:\text{Cd}$ film surface creates negatively charged electron traps, which may be represented as $\text{O}_2 + e^- \rightarrow \text{O}_2^-$, which occurs in the air atmosphere, as shown in the schematic. As a result, a low-conductivity depletion layer forms near the $\text{In}_2\text{S}_3:\text{Cd}$ film surface, resulting in a decreased dark current level. Wang et al. [60] found a similar occurrence in a CuO nanowire photodetector. A photo-produced electron-hole pair is formed on the $\text{In}_2\text{S}_3:\text{Cd}$ film surface when it is exposed to high-intensity light. Desorption of oxygen molecules from the $\text{Cd}:\text{In}_2\text{S}_3$ surface due to recombination of holes with oxygen at the surface can be represented as $\text{O}_2^- + h^+ \rightarrow \text{O}_2$ [61], causing the depletion width to narrow. Meanwhile, photons from incident light are absorbed by valence band (VB) electrons, which are then transferred to the conduction band (CB) [8]. Following that, electrons and holes

from the CB and VB diffuse towards the electrodes. Under light illumination, this process causes an increase in photocurrent. When the light is turned off, oxygen molecules on the film surface are reabsorbed, lowering the current value. In the photodetector based on $\text{In}_2\text{S}_3:\text{Cd}$ film, the amount of recombination of electron-hole pairs is reduced when the applied bias voltage is increased, and the photo-produced charge carriers steadily increase (see Table 2).

4 Conclusions

Using a nebulizer-assisted spray pyrolysis process, an effective Cd-doped In_2S_3 photodetector was manufactured inexpensively. X-ray diffraction examination revealed that Cd-doped In_2S_3 films grew with the preferential orientation along (103) plane, suggesting a raise in the crystallites size. The FESEM investigation showed the presence of a homogenous film. The presence of the constituent elements Cadmium, Indium, and sulfur in the sample was confirmed by EDX analysis. In the ultraviolet area, good light absorption has been developed, and optical investigation has revealed a comparable absorbance in the UV region. As the doping concentration was increased, the optical bandgap decreased from 3.20 to 2.96 eV. $I-V$ characterization revealed an improvement in the current value of 1.06×10^{-6} A for $\text{In}_2\text{S}_3:\text{Cd}$ (4%) thin film. Under UV light, the same film showed a greater photo-response characteristic. $\text{In}_2\text{S}_3:\text{Cd}$ (4%) thin film was found to have a responsivity of 2.12×10^{-1} A/W, the external quantum efficiency of 50%, and a detectivity of 1.84×10^{11} Jones. The current study revealed the considerable impact of Cd doping in In_2S_3 thin films on the structural, optical, morphological, and photodetection characteristics. Hence, the best performing fabricated 4% Cd-doped

Table 3 Comparison table showing the photocurrent, dark current, responsivity, external quantum efficiency, detectivity, Cd-doped In_2S_3 thin films with other reported works

Samples	$I_{\text{photo}}/I_{\text{dark}}$	R (AW ⁻¹)	EQE (%)	D* (Jones)	References
In_2S_3	–	0.213	69	20 E + 9	[54]
1% Sm: CdS	4.9E + 03	1.101	257	2.21E + 12	[55]
CdS:Ga (2%) NR/Au	12E + 03	4	–	–	[56]
CdS:Ag heterojunction	–	0.43	91.42	2.58E + 11	[57]
CdS NB	6	7.43 E + 4	1.9E + 7	–	[58]
5 wt.% Eu: CdS	4.3E + 03	0.614	143	1.38 E + 12	[59]
$\text{In}_2\text{S}_3:\text{Cd}(4\%)$	253	2.12E-01	50.0	1.84E + 11	Present work

In₂S₃ thin film could be better suited for UV light photodetector application.

Acknowledgements

The authors extend their sincere appreciation to the Researchers Supporting Project number (RSP-2021/370), King Saud University, Riyadh, Saudi Arabia for the financial support.

Author Contributions

S: Conceptualization, Data curation, Formal analysis, Writing—original draft, Investigation, Methodology, Resources, Software, Validation, Visualization, and Writing—review and editing. MMI: Conceptualization, Data curation, Formal analysis, Writing—original draft, Investigation, Methodology, Resources, Software, Validation, Visualization, and Writing—review and editing. AMA: Conceptualization, Data curation, Formal analysis, Project administration, Resources, Funding acquisition, Software, Supervision, Validation, Visualization, and Writing—review and editing. MU: Conceptualization, Data curation, Formal analysis, Writing—original draft, Investigation, Methodology, Resources, Software, Supervision, Validation, Visualization, and Writing—review and editing. PA: Conceptualization, Methodology, Resources, Software, Supervision, Validation, Visualization, and Writing—review and editing. BP: Conceptualization, Data curation, Formal analysis, Resources, Software, Supervision, Validation, Visualization, and Writing—review and editing. SFS: Conceptualization, Data curation, Formal analysis, Resources, Software, Supervision, Validation, Visualization, and Writing—review and editing.

Data availability

The raw/processed data required to reproduce these findings cannot be shared at this time as the data also form part of an ongoing study.

Declarations

Conflict of interest The authors report no conflicts of interest.

Supplementary Information: The online version contains supplementary material available at <http://doi.org/10.1007/s10854-022-08766-w>.

5. References

1. H. Nakanishi, *Jpn. J. Appl. Phys.* **19**, 103 (1980)
2. A.V. Kokate, M.R. Asabe, S.D. Delekar, L.V. Gavali, I.S. Mulla, P.P. Hankare, B.K. Chougule, *J. Phys. Chem. Solids* **67**, 2331 (2006)
3. R.R. Sawant, S.S. Shinde, C.H. Bhosale, K.Y. Rajpure, *Sol. Energy* **84**, 1208 (2010)
4. S. Peng, P. Zhu, V. Thavasi, S.G. Mhaisalkar, S. Ramakrishna, *Nanoscale* **3**, 2602 (2011)
5. S. Peng, S.G. Mhaisalkar, S. Ramakrishna, *Mater. Lett.* **79**, 216 (2012)
6. D. Chen, H. Yu, H. Mu, J. Wei, Z. Song, H. Shi, R. Liang, K. Sun, W. Liu, *Carbohydr. Polym.* **94**, 17 (2013)
7. W. Jiang, X. Yin, F. Xin, Y. Bi, Y. Liu, X. Li, *Appl. Surf. Sci.* **288**, 138 (2014)
8. J. Raj Mohamed, C. Sanjeeviraja, L. Amalraj, *J. Mater. Sci. Mater. Electron.* **27**, 4437 (2016)
9. Y. Li, R. Dillert, D. Bahnemann, *Thin Solid Films* **516**, 4988 (2008)
10. M. Kundakci, A. Ateş, A. Astam, M. Yildirim, *Phys. E Low-Dimens. Syst. Nanostructures* **40**, 600 (2008)
11. K.D.A. Kumar, P. Mele, P. Murahari, A.A. Abdeltawab, S.Z. Mohammady, M. Ubaidullah, M.S. Samdani, S. AlFaify, *Sensors Actuators A Phys.* **333**, 113217 (2022)
12. A.V. Kokate, M.R. Asabe, S.B. Shelake, P.P. Hankare, B.K. Chougule, *Phys. B Condens. Matter* **390**, 84 (2007)
13. S.N. Baek, T.S. Jeong, C.J. Youn, K.J. Hong, J.S. Park, D.C. Shin, Y.T. Yoo, *J. Cryst. Growth* **262**, 259 (2004)
14. S.H. You, K.J. Hong, T.S. Jeong, C.J. Youn, J.S. Park, B.J. Lee, J.W. Jeong, *J. Cryst. Growth* **271**, 391 (2004)
15. W. Zhang, H. Yang, W. Fu, M. Li, Y. Li, W. Yu, *J. Alloys Compd.* **561**, 10 (2013)
16. G.F. Epps, R.S. Becker, *J. Electrochem. Soc.* **129**, 2628 (1982)
17. R.R. Sawant, K.Y. Rajpure, C.H. Bhosale, *Phys. B Condens. Matter* **393**, 249 (2007)
18. T. Gnanasekar, S. Valanarasu, I.L. Poul Raj, A.V. Juliet, P.K. Behera, Z.M.M. Mahmoud, M. Shkir, S. AlFaify, *Opt. Mater. (Amsterdam)* **122**, 111790 (2021)
19. P. O'Brien, D.J. Otway, J.R. Walsh, *Thin Solid Films* **315**, 57 (1998)
20. M. Amlouk, M. A. Ben Saïd, N. Kamoun, S. Belgacem, N. Brunet, and D. Barjon, *Japanese J. Appl. Physics, Part 1 Regul. Pap. Short Notes Rev. Pap.* **38**, 26 (1999).

21. T.T. John, M. Mathew, C.S. Kartha, K.P. Vijayakumar, T. Abe, Y. Kashiwaba, *Sol. Energy Mater. Sol. Cells* **89**, 27 (2005)
22. L. Bhira, H. Essaidi, S. Belgacem, G. Couturier, J. Salar-denue, N. Barreaux, J.C. Bernede, *Phys. Status Solidi Appl. Res.* **181**, 427 (2000)
23. R. Jayakrishnan, T.T. John, C.S. Kartha, K.P. Vijayakumar, T. Abe, Y. Kashiwaba, *Semicond. Sci. Technol.* **20**, 1162 (2005)
24. S. Yu, L. Shu, Y. Qian, Y. Xie, J. Yang, L. Yang, *Mater. Res. Bull.* **33**, 717 (1998)
25. R.S. Becker, T. Zheng, J. Elton, M. Saeki, *Sol. Energy Mater.* **13**, 97 (1986)
26. W.T. Kim, W.S. Lee, C.S. Chung, C.D. Kim, *J. Appl. Phys.* **63**, 5472 (1988)
27. N. Kamoun, S. Belgacem, M. Amlouk, R. Bennaceur, J. Bonnet, F. Touhari, M. Nouaoura, L. Lassabatere, *J. Appl. Phys.* **89**, 2766 (2001)
28. R. Diehl, R. Nitsche, *J. Cryst. Growth* **20**, 38 (1973)
29. N. Barreau, J.C. Bernède, S. Marsillac, *J. Cryst. Growth* **241**, 51 (2002)
30. X. Fu, G. Wu, S. Song, Z. Song, X. Duo, C. Lin, *Appl. Surf. Sci.* **148**, 223 (1999)
31. R. Mariappan, V. Ponnuswamy, P. Suresh, *Superlattices Microstruct.* **52**, 500 (2012)
32. I.L.P. Raj, S. Valanarasu, A.A. Abdeltawab, S.Z. Mohammady, M. Ubaidullah, S.F. Shaikh, M. Shkir, *Optik (Stuttg.)* **248**, 168105 (2021)
33. S.S. Kumar Jacob, I. Kulandaisamy, I.L. Poul Raj, A.A. Abdeltawab, S.Z. Mohammady, and M. Ubaidullah, *Opt. Mater. (Amsterdam)*. **116**, 111086 (2021)
34. R. Mariappan, V. Ponnuswamy, P. Suresh, R. Suresh, M. Ragavendar, C. Sankar, *Mater. Sci. Semicond. Process.* **16**, 825 (2013)
35. R. Mariappan, V. Ponnuswamy, M. Ragavendar, *Mater. Sci. Semicond. Process.* **15**, 199 (2012)
36. K.V. Gunavathy, K. Tamilarasan, C. Rangasami, A.M.S. Arulanantham, *Ceram. Int.* **46**, 28342 (2020)
37. K. Otto, P. Bombicz, J. Madarász, I. Oja Acik, M. Krunks, G. Pokol, *J. Therm Anal Calorim* **105**, 83 (2011)
38. D. Nath, F. Singh, R. Das, *Mater. Chem. and Phys.* **239**, 122021 (2020)
39. S. Joishy, S.D. Kulkarni, R.J. Choudary, S.R. Maidur, P. Shankaragouda Patil, B.V. Rajendra, *Mater. Res. Express* **6**, 106447 (2019)
40. K.V. Gunavathy, K. Tamilarasan, C. Rangasami, A.M.S. Arulanantham, *Int. J. Energy Res.* **43**, 7716 (2019)
41. P. Makuła, M. Pacia, W. Macyk, *J. Phys. Chem. Lett.* **9**, 6814 (2018)
42. T. Sall, B. Marí Soucase, M. Mollar, B. Hartitti, M. Fahoume, *J. Phys. Chem. Solids* **76**, 100 (2015)
43. T.T. John, C. Sudha Kartha, K.P. Vijayakumar, T. Abe, Y. Kashiwaba, *Vacuum* **80**, 870 (2006)
44. N. Barreau, S. Marsillac, J.C. Bernède, L. Assmann, *J. Appl. Phys.* **93**, 5456 (2003)
45. W.T. Kim, C.D. Kim, *J. Appl. Phys.* **60**, 2631 (1986)
46. N. Revathi, P. Prathap, R.W. Miles, K.T. Ramakrishna Reddy, *Sol. Energy Mater. Sol. Cells* **94**, 1487 (2010)
47. Y. Zhao, D. Yu, J. Lu, L. Tao, Z. Chen, Y. Yang, A. Wei, L. Tao, J. Liu, Z. Zheng, M. Hao, J. Bin Xu, *Adv. Opt. Mater.* **7**, 1901085 (2019)
48. V.G. Rajeshmon, N. Poornima, C. Sudha Kartha, K.P. Vijayakumar, *J. Alloys Compd.* **553**, 239 (2013)
49. I.L. Poul Raj, S. Valanarasu, K. Hariprasad, J.S. Ponraj, N. Chidhambaram, V. Ganesh, H.E. Ali, Y. Khairy, *Opt. Mater. (Amst)*. **109**, 110396 (2020)
50. B. Hemanth Kumar, M.C. Santhosh Kumar, *Sensors Actuators A Phys.* **299**, 111643 (2019).
51. M. Shkir, I.M. Ashraf, S. AlFaify, A.M. El-Toni, M. Ahmed, A. Khan, *Ceram. Int.* **46**, 4652 (2020)
52. I.L.P. Raj, S. Valanarasu, S. Vinoth, N. Chidhambaram, R.S.R. Isaac, M. Ubaidullah, S.F. Shaikh, B. Pandit, *Sensors Actuators A Phys.* **333**, 113242 (2022)
53. I.J. Tadeo, E.P. Mukhokosi, S.B. Krupanidhi, A.M. Umarji, *RSC Adv.* **9**, 9983 (2019)
54. M. Dharani Devi, A. Vimala Juliet, R.S. Rimal Isaac, M. Ramudu, V. Ganesh, Y. Bitla, I.S. Yahia, *J. Elec. Mater.* **50**, 4373 (2021)
55. M. Shkir, I.M. Ashraf, A. Khan, M. Taukeer Khand, A. Mohamed El-Tonic, S. AlFaify, *Sens. Actuators A Phys.* **306**, 111952 (2020)
56. D. Wu, Y. Jiang, Y. Zhang, Y. Yu, Z. Zhu, X. Lan, F. Li, C. Wu, L. Wang, L. Luo, *J. Mater. Chem.* **22**, 23272 (2012)
57. N. I. Najm, H. K. Hassun, B. K. H. Al-Maiyaly, B. H. Hussein, and A. H. Shaban in *AIP Conf. Proc.* (2019), p. 020031.
58. L. Li, P.C. Wu, X.S. Fang, T.Y. Zhai, L. Dai, M.Y. Liao, Y. Koide, H.Q. Wang, Y. Bando, D. Colberg, *Adv. Mater.* **22**, 3161 (2010)
59. M. Shkir, I.M. Ashraf, K.V. Chandekar, I.S. Yahia, A. Khan, H. Algarni, S. AlFaify, *Sensors Actuators A Phys.* **301**, 111749 (2020)
60. S.B. Wang, C.H. Hsiao, S.J. Chang, K.T. Lam, K.H. Wen, S.C. Hung, S.J. Young, B.R. Huang, *Sensors Actuators A Phys.* **171**, 207 (2011)
61. W. Yin, J. Yang, K. Zhao, A. Cui, J. Zhou, W. Tian, W. Li, Z. Hu, J. Chu, *A.C.S. Appl. Mater. Interfaces* **12**, 11797 (2020)

Publisher's Note Springer Nature remains neutral with regard to jurisdictional claims in published maps and institutional affiliations.

Springer Nature or its licensor holds exclusive rights to this article under a publishing agreement with the author(s) or other rightsholder(s); author self-archiving of the accepted

manuscript version of this article is solely governed by the terms of such publishing agreement and applicable law.